A Study on Internal Erosion of Low-Plasticity Silty Sand

Jing-Wen Chen[1], Bo-Rung Lin[2], Wei F. Lee[3] and Yie-Ruey Chen[4]
[1,2]*Department of Civil Engineering, National Cheng Kung University, Tainan, Taiwan*
[3]*Ground Master Construction Co., Ltd., Taipei, Taiwan*
[4]*Department of Land Management and Development, Chang Jung Christian University, Tainan, Taiwan*
E-mail: geochen@mail.ncku.edu.tw

ABSTRACT: Internal erosion phenomenon of low plasticity silty sand causing by migrant of fines content within soil matrix is of great interest to engineers. A novel direct shear device was developed to enable controlled seepage flows to be introduced during testing. In this study, this new developed seepage flow direct shear test device was used to investigate the effects of internal erosion to non-plastic silty sand prior to shearing. Specimens prepared with different fines contents and relative densities were tested to examine the influences of fines and density state to planar shear strength of non-plastic silty sand after experiencing internal erosion.
The results revealed that coarse particles existing in the test specimens still dominate the behavior of soil. Hence, when all soil specimens had similar void ratios, the strength of the eroded soil is greater than that of the uneroded soil ones. Moreover, fines contents had noticeable influence on soil behaviors, regardless of whether an internal erosion process was applied to the samples. Results of presented study is hoped to improve engineers' understandings in engineering behavior of low plasticity silty sand.

KEYWORDS: Seepage flow direct shear (SFDS) device, Fines content, Friction angle, Low plasticity silty sand

1. INTRODUCTION

Recently, internal erosion phenomenon of low plasticity silty sand causing by migrant of fines within soil matrix has been of great research interest in geotechnical engineering. Thevanayagam (1998) stated that a fine soil particle with a diameter ratio R_d (R_d = D/d; D: diameter of a coarse soil particle; d: diameter of a fine soil particle) >6.5 can freely travel among the voids of coarse soil particles. Lade et al. (1998) classified soil particles into three phases (filling-of-voids phase, transition zone phase, and replacement-of-solids phase) according to soil fines content. The filling-of-voids phase represents soils with a fines content in the range of 0%–25%. The transition zone phase pertains to soils with a fines content in the range of 25%–35% and features the smallest soil porosity. Finally, the replacement-of-solids phase represents soils with a fines content larger than 35%. These phases indicate that increasing fines content causes soil porosity to decrease initially and then increase; furthermore, fines no longer serve as void fillers in the soil structural arrangement of the transition phase, and instead to start serving as the main structural component. The described phase transformation is an essential factor when analyzing engineering behavior of low plasticity silty sand. Yamamuro and Lade (1999) proposed the following hypothesis regarding soil particle fabric: at a constant soil volume, when the voids within a sandy soil structure are filled, the overall soil density increases, but the sliding behavior of coarse particles in the soil is not affected. In other words, adding fines to a sandy soil structure only slightly affects the behavior of its coarse particles. Yamamuro and Covert (2001) confirmed that an excessively high fines content over transition phase facilitates adsorbing fines onto the surface of coarse particles, separating the contact surface between the coarse particles. Furthermore, Yamamuro and Covert (2001) examined a two-stage effect of fines content on the particle fabric of a dense soil sample. They confirmed that at a constant soil volume, fines added to the soil sample tend to first fill the voids between the existing coarse particles and reduce soil porosity. Subsequently, adding sufficient fines to the soil sample causes the soil porosity to reach the critical point, or the minimum soil porosity. However, once the critical point is exceeded by adding additional fines, the soil porosity starts to increase. Kokusho and Fujikura (2008) used a conventional constant-head seepage test apparatus to investigate the effects of hydraulic gradient and flow velocity on the loss of soil grains in soil samples under a seepage condition. The results indicated that the unevenness of the grains within the poorly graded soil reduced the friction between the grains. Therefore, a water flow easily eroded the soil grains, and the seepage rate rapidly increased in the loose soil grains. The research group first developed a Flexible Wall Pinhole Test Device, FWPD, to investigate the internal erosion features of non-plastic silty sand (Chen, 2012; Lee et al., 2013, 2014). The FWPD was designed to allow pinhole erosion tests to be conducted under various controlled confining pressure. Test results of FWPD revealed that low plasticity fines could be washed out through seepage channel introduced by a pinhole even under high confining pressure. It was found that confining pressure, initial state of density, and seepage velocity are major influence factors to the internal erosion behavior of non-plastic silty sand. However, post internal erosion strength properties of low plasticity silty sand have not been well studies due to the limitation of proper testing device that could allow internal erosion and loading tests to be conducted on the same specimen.

In an effort to further investigate internal erosion behavior and its effects to engineering properties of low plasticity silt sand, a new direct shear device, Seepage Flow Direct Shear Device, SFDS, was developed by Lee and Ishihara (2010). Further expanding the research scope from FWPD, the SFSD was designed to allow controlled seepage to flow through entire cross section of test specimens, therefore, planar strength of low plasticity silty sand before, during, and after internal erosion could be examined. In this study, specimens prepared with different fines contents and relative densities were tested to examine the influences of fines and density state to planar shear strength of non-plastic silty sand after experiencing internal erosion. The results revealed that coarse particles existing in the test specimens still dominate the behavior of soil. Hence, when all soil specimens had similar void ratios, the strength of the eroded soil is greater than that of the uneroded soil ones.

2. SEEPAGE FLOW DIRECT SHEAR DEVICE

Figure 1 shows the schematic drawing and photo of the developed Seepage Flow Direct Shear device, SFDS. It was developed by modifying the conventional 120*mm* diameter circular shear box direct shear device. Top cap of the shear box was designed to allow seepage flow to seeping through the specimen. As shown in Figure 2 (top cap photo), four water inlets are installed on top cap and a porous stone is attached to the top cap to ensure seepage water to be evenly introduced to flush the entire cross section of the test specimen. The shear box was modified to accommodate rubber membrane to be used within the shear box so as to secure the seepage to flow through the specimen while shearing. The lower cap of the shear box is also modified to allow seepage water and fines to be collected after flushing out from the specimen (Figure 2). In addition, a water supply system was designed to provide de-aired

water for saturating the specimen and maintain constant flow of seepage water under regulated pressure as shown in Figure 3. Both axial load and horizontal load capacities of SFDS were designed as 1000kgf. The axial load is applied by two vertical air cylinders, and horizontal load is applied by mechanical crew system. Two load cells and two LVDT are equipped to measure vertical and horizontal loads and displacements. The maximum overburden pressure that SFDS could simulate is in a range of 8 to 8.5kgf/cm^2.

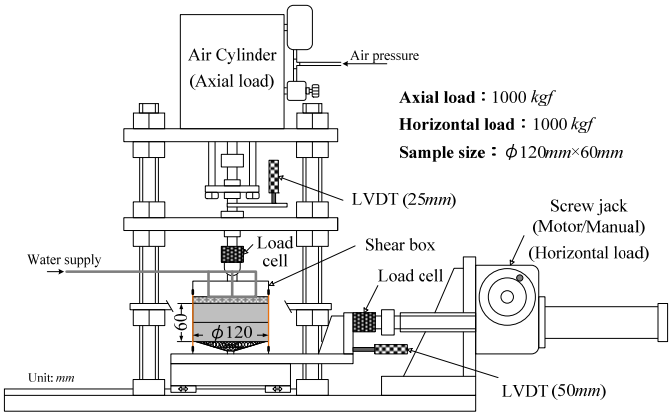

Figure 1 Configuration of the SFDS apparatus

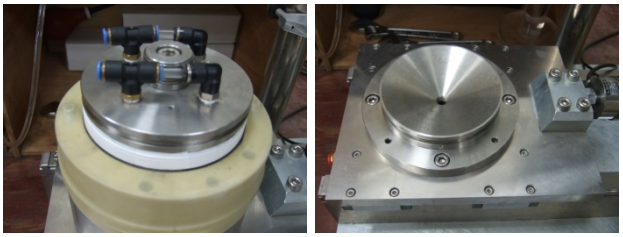

Figure 2 Top cap and lower base of the direct shear box

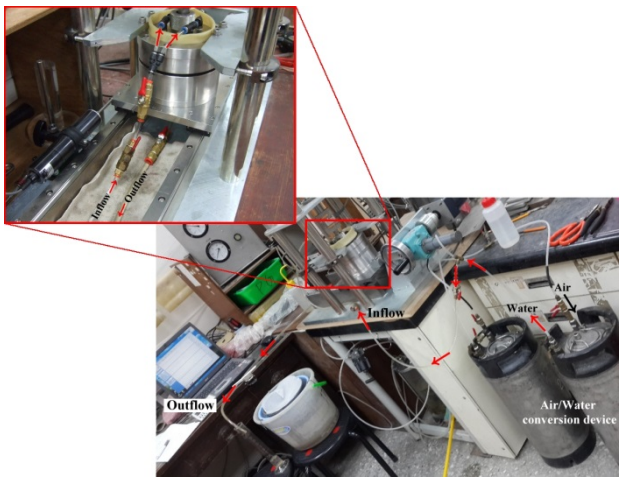

Figure 3 Water supply system

3. SOIL SAMPLE AND TEST PROCEDURES

In the current study, a typical local low plasticity silty sand, Li-Gang sand, was obtained and used as the representative soil sample. Specifically, the sampling site, Li-Gang, is located in the basin of the Laonong River, a main tributary of the Gaoping River (Figure 4). Li-Gang sand is a type of gray silty sand with a specific weight, coefficient of uniformity (C_u), coefficient of curvature (C_c), and liquid limit (LL) of 2.66, 5.5, 0.89, and 24, respectively, as listed in Table 1. It is categorized as poorly graded soil. Index properties of test specimens with dissimilar fines contents are also listed in the table. Figure 5 illustrates the particle size distribution curves of original Li-Gang sand and remolded samples prepared with various fines contents obtained using sieve analysis and hydrometer analysis. As shown in Table 1, both maximum and minimum void ratios of the test samples increased as the fines contents increased.

Table 1 Physical Properties of the In-situ Soil Samples and the Remolded Samples with Dissimilar FC

	In-situ Soil Samples	Remolded Soil Samples		
FC (%)	2.21	10	20	30
G_s	2.66	2.68	2.72	2.81
$\gamma_{d,max}$ (g/cm^3)	-	1.959	1.932	1.856
$\gamma_{d,min}$ (g/cm^3)	-	1.505	1.462	1.401
e_{max}	-	0.779	0.857	1.003
e_{min}	-	0.367	0.405	0.512
D_{60} (mm)	1.2	1.065	0.92	0.73
D_{50} (mm)	0.85	0.75	0.7	0.485
D_{30} (mm)	0.48	0.39	0.28	0.0738
D_{10} (mm)	0.218	0.074	0.01	0.00226
C_u	5.50	14.39	92.00	323.01
C_c	0.89	1.93	8.52	3.30
USCS	SP	SM	SM	SM

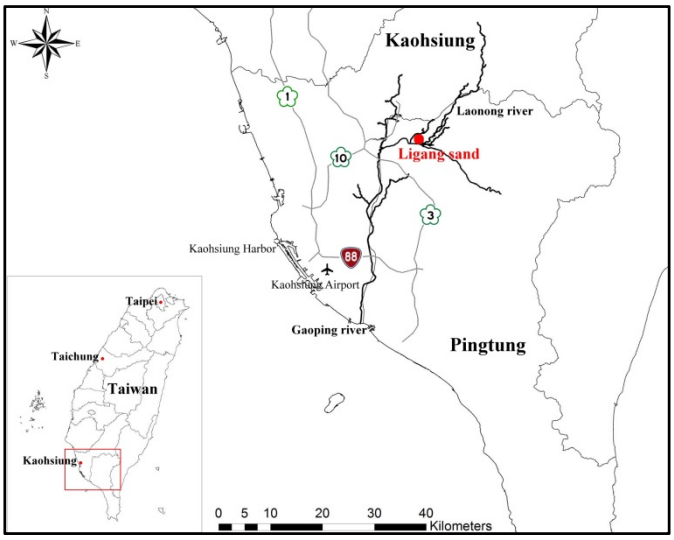

Figure 4 Location of the Ligang site

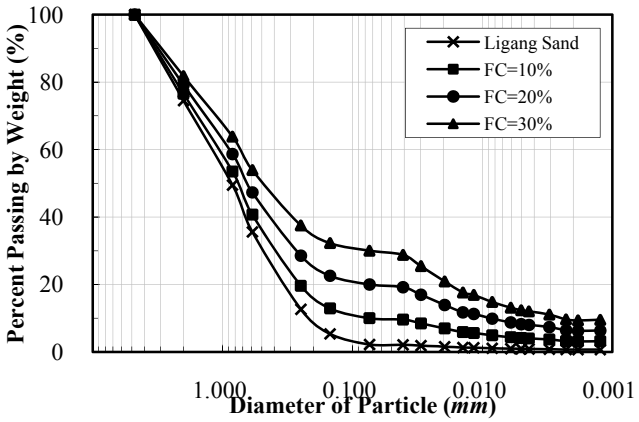

Figure 5 Particle size distribution curves of the undisturbed and remolded samples

The controlled relative density (D_r) and fines contents for test sample preparation are D_r=30% and FC=10%, 20%, or 30% accordingly. Test samples were prepared directly within the shear box with membrane fixed on the edge of shear box. Once the fines content washed out during shear testing, filter stones and ϕ2-*mm* filter, which was laid on lower base of the direct shear box (Figure 2), will avoid clogging of the filter inside the outflow pipe. Moisture tamping method (Ishihara, 1993), was used to prepare the test samples, which was placed in five layers by tamping each layer with the help of a hammer. Two ring spacers, 5*mm* in thickness, are placed in-between upper and lower portions of shear box to assist specimen preparation (Figure 6). The main function of the ring spacer is to form a spacing with 5*mm* thick by taking it apart after the saturated specimen was consolidated by applying vertical loads and before conducting the internal erosion test.

During preparation process, carbon dioxide was introduced into the specimen to force out the air in the voids before saturating the specimen to accelerate saturation process. Subsequently, the saturated specimen was consolidated by applying vertical loads. Volumetric changes or post-consolidation void ratio of the test specimen could be measured or calculated by discharged pore water or vertical displacement. After the consolidation was completed, pressurized de-aired water was then introduced into the specimen from the inlets on top cap of the shear box to conduct the internal erosion test. The seepage water was collected using graduated cylinders after flushing through the specimen. Overall permeability could be estimated by the total volume of outflow seepage water and duration of collection. The erosion test was set to start with an initial back pressure of 10 *kPa*. The water pressure was then increased by a 10-*kPa* increment. Each pressure increment was held for at least 15min to allow internal erosion to be developed and then completed, i.e. the seepage water became transparent again. The test was then terminated when the water pressure reaches the confining pressure level applied on the specimen via vertical load. Usually, two types of internal erosion phenomena were observed. Figure 7 shows the result of test of which specimen was prepared at a relative density of 30% and a fines content of 10% at the condition under 100 *kPa* overburden pressure and 10 *kPa* seepage pressure. As shown in the figure, the collected seepage water immediately turned dark at the beginning of the test, and the turbid water kept coming out for about two minutes before it turned to transparent. Figure 8 shows another type of test results. The seepage water collected started transparent, and then become lightly turbid, if internal erosion developed, and finally become transparent again at the end of each increment. This usually occurred at tests of which specimens have higher fines contents, in a range of 20% to 30%, and was conducted under high overburden pressure.

To conduct the shear test, two ring spacers were removed prior to shearing to allow free particle movement, as shown in Figure 9. The shear tests were conducted at a horizontal rate of 1.5*mm*/min, and the maximum horizontal strain was set at 10% of the diameter. Measurements including vertical load, horizontal load, vertical displacement, and horizontal displacement, were recorded every 10 seconds. After the test, the specimen was cut separately into upper, middle, and lower layers and dried in a laboratory oven. Grain size distribution analysis were then conducted to investigate remaining fines contents.

In this study, on site bulk Li-Gang sand with a 30% fines content was used to conduct several verification tests. The specimen was prepared at a relative density of 30%. Test was conducted at overburden pressure of 100*kPa* with a maximum seepage water pressure of 100*kPa*. In addition to sampling fines contents at upper, middle, and lower layers of the test specimens, inner and outer portions of the same layer of test specimens were also compared to check if the seepage flow could evenly flush the entire cross section of the test specimens (Figure 10). Table 2 shows a typical result of the verification tests. As shown in the table, results of the post-test sieve analyses indicate that inner and outer portions have similar fines contents, meaning the seepage flow evenly flushed through the specimen. It was observed that both upper and lower layers have lower fines contents than that of the middle layer. This phenomenon indicates that particle crushing likely occurred during the shearing and had created more fines along the shearing plane.

Table 2 Percentage Values of the FC Obtained through the Sieve Analysis

	Inner Circle	**Outer Ring**
Upper layer	24.29%	25.53%
Medium layer	27.48%	27.81%
Lower layer	25.34%	23.66%

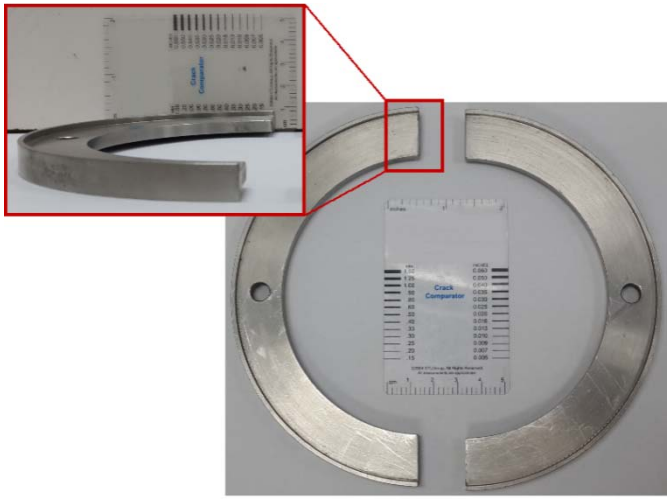

Figure 6 Half-moon-shaped ring spacers (D=5*mm*)

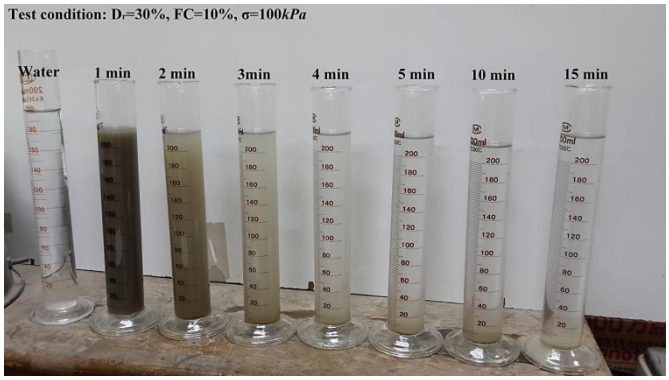

Figure 7 Solutions drained from the specimen with 10% FC

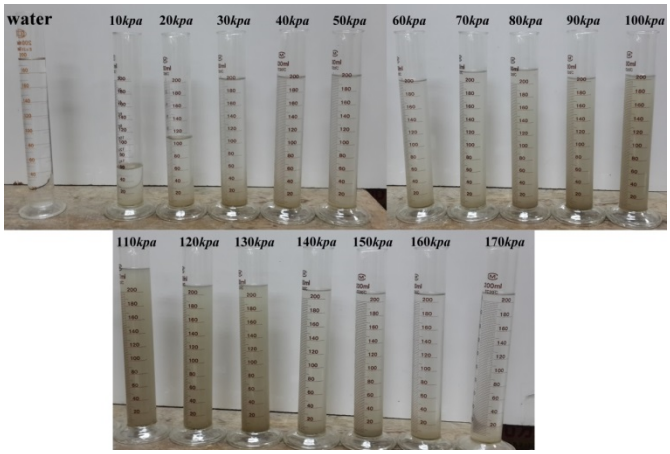

Figure 8 Solutions drained from the specimen with 20%–30% FC (Each erosion stage lasted 15 min)

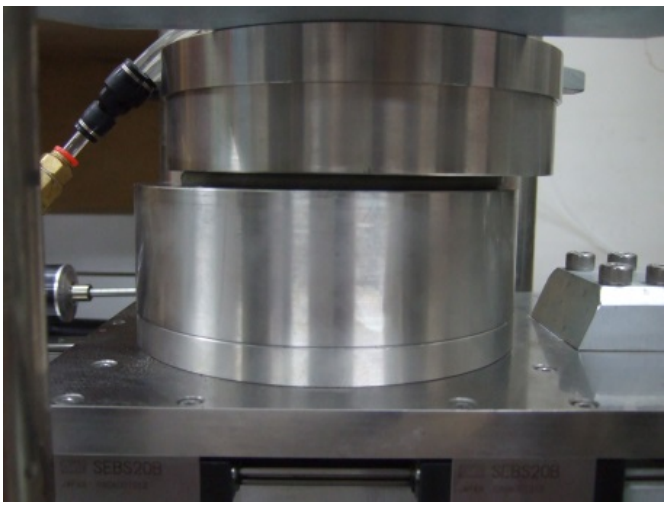

Figure 9 Shear test process and the shear surface (D=5*mm*)

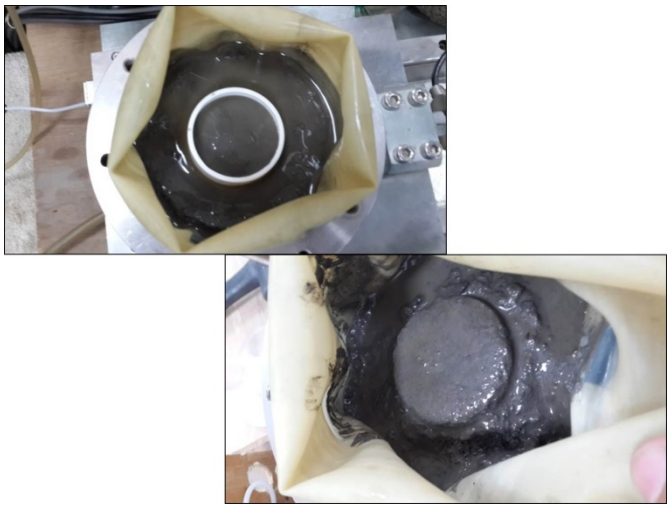

Figure 10 Inner circle and outer ring portions of the soil sample

4. COMPARISON OF THE TEST RESULTS OBTAINED THROUGH THE CONVENTIONAL DIRECT SHEAR DEVICE AND THE SFDS DEVICE

Direct shear tests were firstly conducted using both conventional direct shear device and SFDS device in an effort to confirm the SFDS device is adequate of performing direct shear tests. Despite the size difference of shear boxes between two types of direct shear devices, test specimens prepared at a 30% relative density with fines contents of 10%, 20%, or 30%. Three levels of vertical pressure, 100, 300, or 500 *kPa* were applied. The gap between top and lower caps of shear boxes were both set to be zero in this series of tests.

Table 3 shows a summary of the void ratio (e), friction angle (ϕ), and volumetric strain (ε_v) values obtained using the DS and SFDS instruments under the various test conditions. Figure 11 illustrates the correlations between the void ratio and friction angle values acquired using the two instruments. In this figure, the solid, hollow symbols and, diagonally hatched symbols represent the test values obtained under 100, 300, and 500 *kPa*, respectively; the square and circular symbols represent the test values obtained through the DS and SFDS instruments (D=0*mm*), respectively; the black solid and dash lines are the linear regression curves of the test results acquired using the DS and SFDS instruments, respectively. According to the results, the void ratios and friction angles obtained through the DS apparatus were 0.606–0.342 and 27.0˚–35.0˚, respectively. The void ratios and friction angles obtained through the SFDS apparatus were 0.671–0.437 and 27.9˚–33.0˚, respectively. The test results of both instruments indicated that the average void ratio decreased with the normal force. By contrast, the average friction angle increased as the average void ratio decreased. Table 3 and Figure 11 summarizes the test results. The results had confirmed that SFDS device is capable of performing direct shear tests and the test results could be used to discuss strength properties of previous results obtained by conventional direct shear tests.

Table 3 Void Ratio, Friction Angle, and Volumetric Strain Obtained Using the Two Different Instruments

DS Test									
FC(%)	10			20			30		
σ(*kPa*)	100	300	500	100	300	500	100	300	500
e	0.539	0.418	0.342	0.536	0.452	0.423	0.606	0.569	0.519
ϕ (°)	27.0	28.6	35.0	30.0	30.2	34.0	27.5	29.5	30.3
ε_v (%)	1.25	3.03	4.30	1.63	2.89	2.10	0.90	2.00	1.60
SFDS Test (*D* = 0 *mm*)									
FC(%)	10			20			30		
σ(*kPa*)	100	300	500	100	300	500	100	300	500
e	0.536	0.455	0.437	0.587	0.496	0.500	0.671	0.632	0.614
ϕ (°)	32.4	33.0	32.5	31.7	31.4	32.0	27.9	28.8	31.6
ε_v (%)	2.74	3.13	3.65	1.99	2.61	2.72	1.51	1.84	1.82

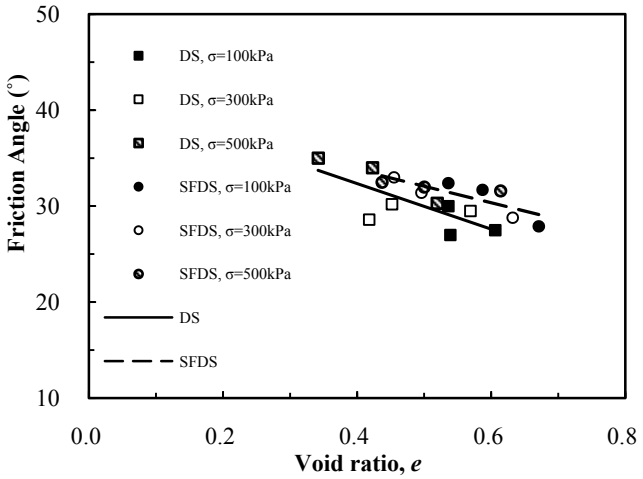

Figure 11 Correlations between the void ratio and friction angle obtained using the two different instruments (D=0*mm*)

5. RESULTS OF THE SFDS TEST

The remolded soil samples created from Ligang sand were used to conduct the SFDS tests. When the relative density was 30% and shear gap was 5*mm*, various normal force magnitudes (100, 300, and 500 *kPa*) were exerted on the soil samples (FC = 10%, 20%, or 30%) with or without applying an erosion condition. Table 4 summarizes the void ratio before (e) and after (e_e) the erosion process, friction angle (ϕ), and volumetric strain (ε_v) of the consolidated samples obtained using the SFDS apparatus. The nonerosion–shear test results revealed that the void ratios of the consolidated remolded samples ranged from 0.692 to 0.467. The erosion–shear test results indicated that the void ratios of the consolidated remolded samples before and after the erosion process were 0.736–0.463 and 0.703–0.461, respectively. The results of tests under the two conditions indicated that the average void ratio increased as the normal force decreased. Moreover, the average volumetric strain of the sheared samples was directly related to the normal force. By contrast, the average friction angle within the samples was inversely related to the average void ratio.

Table 4 Void Ratio, Friction Angle, and Volumetric Strain of the Samples Derived from the Nonerosion–shear Test and Erosion–shear Test

Nonerosion–shear test (*D* = 5 *mm*)									
FC(%)	10			20			30		
σ(*kPa*)	100	300	500	100	300	500	100	300	500
e	0.562	0.533	0.467	0.610	0.554	0.522	0.692	0.648	0.601
ϕ(°)	22.0	27.1	27.4	20.3	23.3	26.4	15.7	16.9	24.5
ε_v (%)	2.52	2.88	2.95	1.41	1.62	1.65	0.84	1.20	1.15
Erosion–shear test (*D* = 5 *mm*)									
FC(%)	10			20			30		
σ(*kPa*)	100	300	500	100	300	500	100	300	500
e	0.580	0.531	0.463	0.556	0.533	0.509	0.736	0.640	0.633
e_e	0.541	0.525	0.461	0.578	0.527	0.484	0.703	0.611	0.625
ϕ(°)	27.4	28.0	28.2	20.3	25.1	27.3	17.3	19.8	24.5
ε_v (%)	2.74	2.91	3.14	1.67	2.33	2.43	1.01	1.11	1.46

Figure 12 shows correlations among the shear stress, horizontal strain, and vertical strain of the SFDS test samples with shear gap D=5*mm* and FC=10%. Normal stresses of 100*kPa*, 300 *kPa*, and 500 *kPa* are represented by solid line, dashed line, and dot-dashed line, respectively. Thin lines correspond to the nonerosion–shear test and thick lines correspond to the erosion–shear test. All tests in this study are according to ASTM specification (2011). The shear strength of the soil is the shear stress corresponding to shear strain 10% when the rubber membrane still keeps its integrity. Using the test results corresponding to three different normal stresses, we obtain Mohr-Coulomb failure envelope. The envelope is tangent to the Mohr circles representing failure conditions. The results show that the variation of stress-strain curve is not obvious regardless of whether the soil erosion when normal stress is getting bigger. When normal stress is getting smaller, shear strength of the erosion–shear test sample is larger than that of the nonerosion–shear one. In other words, shear strength of the soil increases after erosion because coarse particulates dominate.

Figure 13 illustrates the correlations between the FC and friction angles of the samples tested using the SFDS (D=5*mm*) apparatus. In this figure, the square, circular, and triangular symbols represent the values obtained under a normal force condition of 100, 300, and 500 *kPa*, respectively; the solid and hollow symbols represent the values acquired in the nonerosion–shear test and erosion–shear test, respectively. The results revealed that the friction angles ranged from 15.7˚ to 28.2˚ and were directly correlated with the normal force. Figure 14 illustrates the correlations between the FC and the shear strength values. Same as Figure 12, the shear strength of the soil is the shear stress corresponding to shear strain 10%. The symbols in this figure represent the same items as those described in Figure 13. The results showed that the shear strength of the eroded and sheared samples was greater than that of the uneroded and sheared samples. This finding indicates that applying an erosion process to a soil sample removes its soil particles and alters its soil fabric, thereby modifying its mechanical behavior.

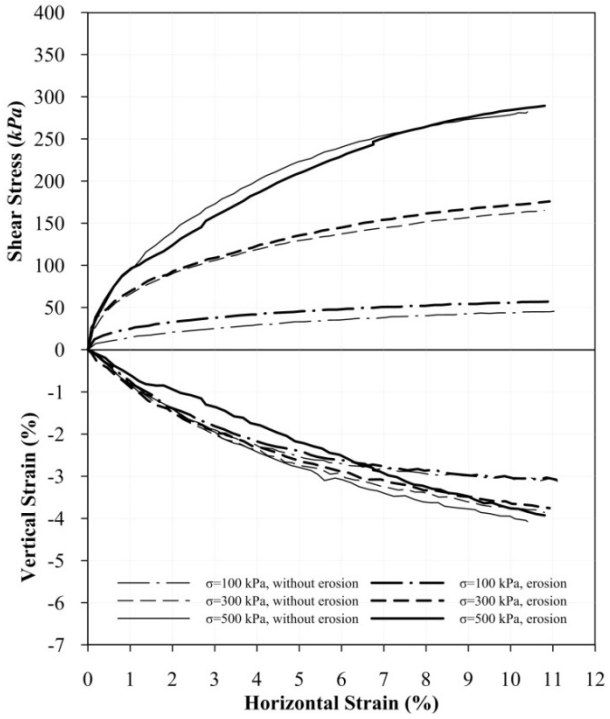

Figure 12 Correlations among the shear stress, horizontal strain, and vertical strain of the SFDS test samples (D=5*mm*, FC=10%)

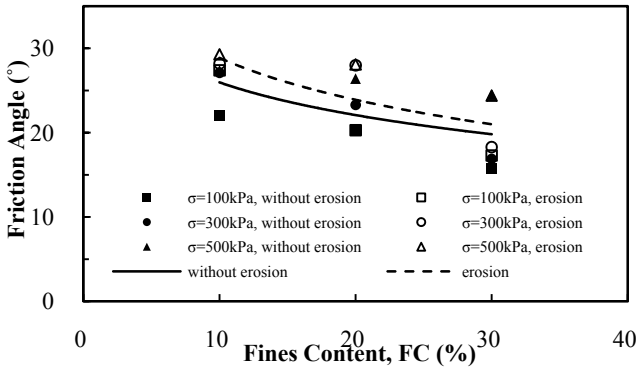

Figure 13 Correlations between the FC and friction angles of the samples tested using the SFDS apparatus

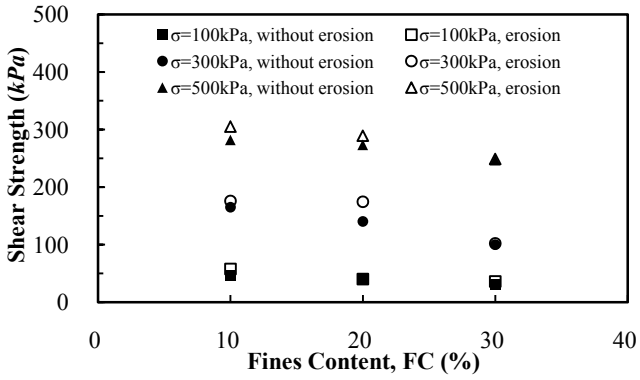

Figure 14 Correlations between the FC and shear strength of the SFDS test samples

5.1 Correlations of void ratios, friction angles, and shear strength

Figure 15 illustrates the correlations between the void ratios and friction angles, and Figure 16 depicts the correlations between the void ratios and shear strength (D_r=30%, D=5*mm*). In these figures, the square, circular, and triangular symbols represent the test values obtained under a normal force condition of 100, 300, and 500 *kPa*, respectively; the solid and hollow symbols represent the values acquired in the nonerosion–shear test and erosion–shear test, respectively. The results indicated that the internally eroded soil samples predominantly comprised coarse particles. Hence, under the condition of similar void ratios, the friction angles of the eroded soil samples were higher than those of the uneroded soil samples. Furthermore, the void ratios and friction angles of the soil samples were inversely correlated. The normal force was also inversely correlated with the void ratios, but it was directly correlated with the shear strength.

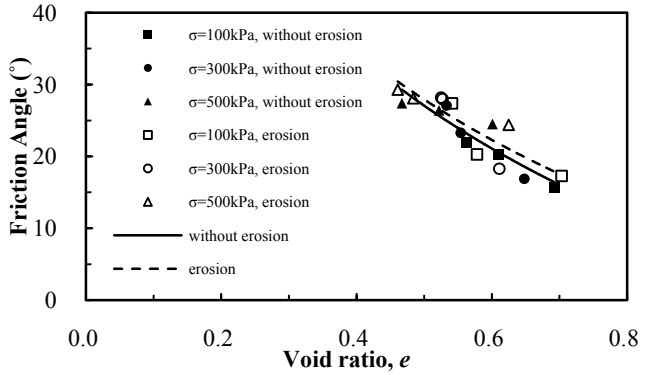

Figure 15 Correlations between the void ratios and friction angles of the SFDS test samples

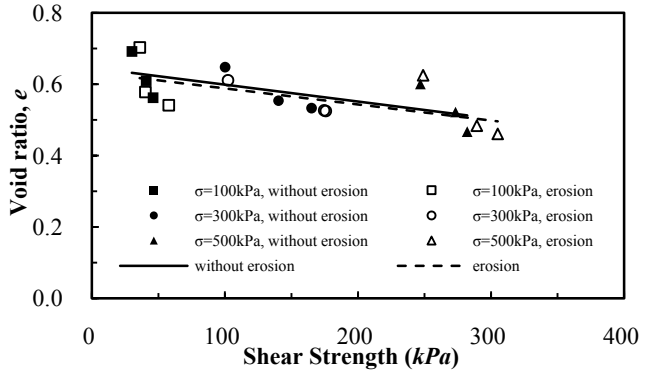

Figure 16 Correlations between the void ratios and shear strength of the SFDS test samples

5.2 Correlations of void ratios, volumetric strain, and variations in the FC

Figure 17 shows the correlations between the void ratios and volumetric strain of the samples. In this figure, the square, circular, and triangular symbols represent the test values obtained under a normal force condition of 100, 300, and 500 *kPa*, respectively; the solid and hollow symbols represent the values acquired in the nonerosion–shear test and erosion–shear test, respectively. The results indicated that the eroded soil samples exhibited large pores. Hence, the volumetric strain of the eroded and sheared samples was greater than that of the uneroded and sheared samples.

Figure 18 depicts the correlations between the void ratios and changes in the FC of the samples. The symbols in this figure represent the same items as those described in Figure 17. The changes in the FC were defined as the percentage difference between the FC of a remolded sample before and after the SFDS test. In the nonerosion–shear test, this difference signified the increment of fine-grained particles in a sample after the sample was sheared. In the erosion–shear test, this difference represented the variation in the FC of a sample after the sample was eroded and sheared.

The results revealed that the variations in the FC of the uneroded and sheared samples as well as the eroded and sheared samples were approximately 1%–2.5% and 1.5%–7%, respectively. Moreover, regardless of whether the erosion process was applied to the samples, the variations in the FC increased with the void ratios. The changes in the FC of the eroded and sheared samples were also considerably greater than those of the uneroded and sheared samples.

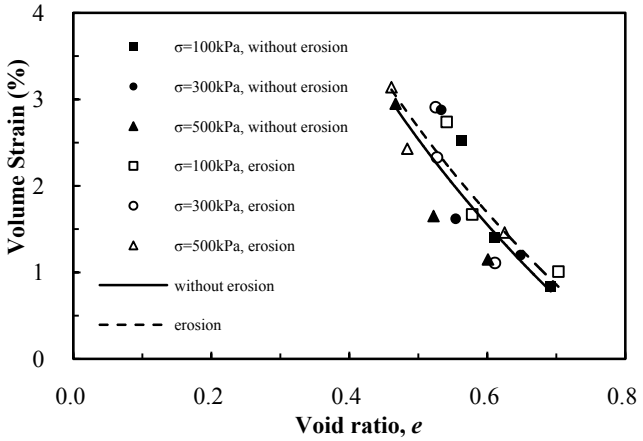

Figure 17 Correlations between the void ratios and volumetric strain of the SFDS test samples

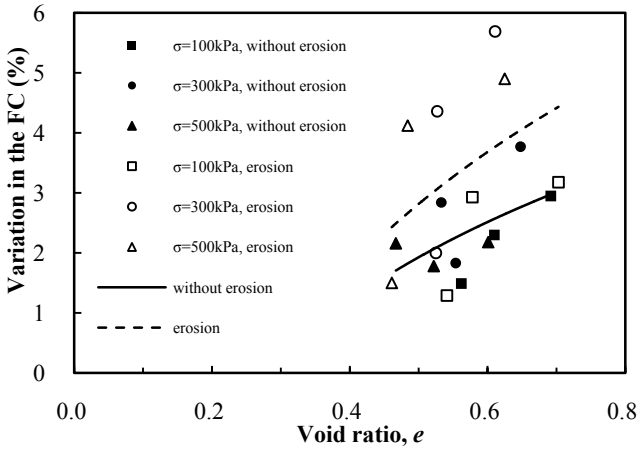

Figure 18 Correlations between the void ratios and variations in the FC of the SFDS test samples

5.3 Erosion water pressure, flow velocity, and time

Figure 19 shows the correlations between the erosion water pressure and flow velocity (internal erosion velocity). In this figure, the solid, dash, and dash–dot line represent the test values acquired under a normal force condition of 100, 300, and 500 *kPa*, respectively; the black, blue, and red lines represent the test values obtained at 10%, 20%, and 30% FC, respectively. Because the soil samples used in this study were classified as low-plasticity silty sand, the samples with a 10% FC exhibited a maximum flow velocity of 4.02×10^{-2} *cm/s*. The samples with a 20% or 30% FC demonstrated flow velocities ranging from 1.22×10^{-2} to 3.79×10^{-3} *cm/s*. These results indicate that the seepage velocities are inversely related to the FC and normal force.

Figure 20 illustrates the correlations between the permeability coefficients and time. The lines in this figure represent the same items as those described in Figure 19. The permeability coefficients observed when the FC was 10% were higher than those observed when the FC was 20% or 30%. This difference is attributed to how the seepage flows were disturbed during the erosion process (Figures 7 and 8). When the FC was set to 10% FC and erosion

water pressure was set to 10 *kPa*, a highly turbid drained solution was immediately produced. Consequently, the seepage coefficient peaked at the beginning of the test and then decreased as the time increased. When the FC of the samples increased to 20% and 30%, the resulting drained solutions became turbid as the erosion water pressure increased. Therefore, the permeability coefficients and erosion water pressure were directly correlated. However, regardless of the amount of FC, the permeability coefficients increased with the erosion water pressure. Moreover, the permeability coefficients remained constant once they peaked.

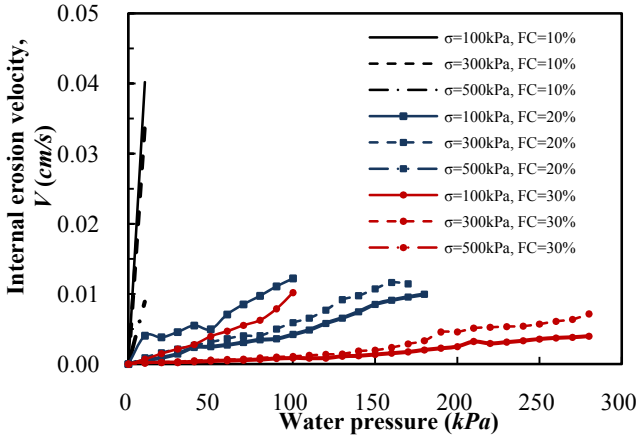

Figure 19 Correlations between the erosion water pressure and flow velocity

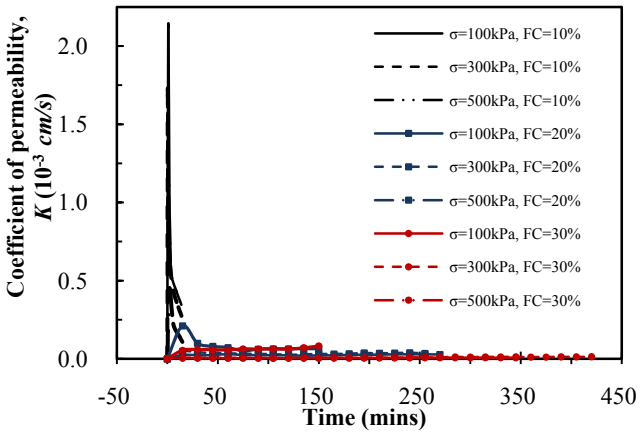

Figure 20 Correlations between the coefficients of permeability and time

6. CONCLUSIONS

In this study, an SFDS apparatus was developed for investigating the behaviors of low-plasticity silty sand. Ligang sand was used to create remolded soil samples. Test conditions involving various magnitudes of normal force and varying FC were adopted to simulate and investigate the effect of internal erosion on the characteristics of fine-grained soil particles. The test results are listed as follows:

1. SFDS device with rubber membrane, can measure the volume change of the erosion–shear test sample with considerable speed as the advantage of traditional direct shear device. Furthermore, SFDS device combines with seepage test to explore the soil erosion behavior under seepage flows.
2. The results of the DS and SFDS tests indicated that the average void ratio of the samples with varying FC decreased as the normal force increased. After the samples were sheared in the SFDS test, the volumetric strain of the samples was found to be directly correlated with the normal force. By contrast, the average void ratios and friction angles were inversely correlated.
3. The internally eroded soil samples mainly comprised coarse particles. Hence, under the condition of similar void ratios, the friction angles of the eroded soil samples were greater than those of the uneroded samples. The friction angles also decreased as the void ratios increased.
4. Regardless of whether an internal erosion process was applied, the FC of the samples increased with the void ratio. Furthermore, the sheared soil samples with a high FC exhibited a high variation in their particle size distribution, low soil variation ratio, and small friction angle.
5. The results of the internal erosion test indicated that the seepage flow velocities decreased as the FC and normal force increased. Moreover, regardless of the FC of the samples, the permeability coefficients increased as the erosion water pressure increased. After the permeability coefficients peaked, they remained constant as the time increased.

7. ACKNOWLEDGMENTS

This study was supported and funded by the Ministry of Science and Technology, Taiwan (MOST 103-2627-B-006-004). Additionally, Prof. Kenji Ishihara and Prof. Takaji Kokusho of the Chuo University provided assistance and guidance in developing the apparatus and conducting the tests, and the graduate students from the Laboratory of Marine Geotechnology, National Cheng Kung University, participated in the preliminary tests.

8. REFERENCES

ASTM D3080M-11, (2011) Standard test method for direct shear test of soils under consolidated drained conditions, ASTM International, West Conshohocken, PA. doi:10.1520/D3080_D3080M-11

Chen, C. C., (2012) "Study on Engineering Properties of Low-Plasticity Silty Sand ", PhD dissertation. Department of Civil Engineering, National Cheng Kung University, Tainan, Taiwan.

Ishihara, K., (1993) "Liquefaction and flow failure during earthquakes", Geotechnique, Vol. 43, No. 3, pp 315-415. doi:10.1680/geot.1993.43.3.351

Kokusho, T. and Fujikura Y., (2008) "Effect of particle gradation on seepage failure in granular soils", Fourth international conference on scour and erosion, pp. 497-504.

Lade, P. V., Liggio, C. D. and Yamamuro, J. A., (1998) "Effects of non-plastic fines on minimum and maximum void ratios of sand", ASTM Geotechnical Testing Journal Vol. 21, No. 4, pp 336-347.

Lee, W. F. and Ishihara, K., (2010) Personal communications.

Lee, W. F., Chen, C. C., Chen, J. W. and Ishihara, K., (2013) "Engineering Properties of Non-Plastic Silty Sand", Sound Geotechnical Research to Practice, pp 420-430.

Lee, W. F., Chen, C. C., Chen, J. W. and Ishihara, K., (2014) "Liquefaction Potential of Non-Plastic Silty Sand", Journal of Marine Science and Technology, Vol. 22, No. 2, pp 137-145.

Thevanayagam, S., (1998) "Effect of fines and confining stress on undrained shear strength of silty sands", Journal of Geotechnical and Geoenvironmental Engineering Vol. 124, No. 6, pp 479-491.

Yamamuro, J. A. and Lade, P. V., (1998) "Steady-state concepts and static liquefaction of silty sands", Journal of Geotechnical and Geoenvironmental Engineering Vol. 124, No. 9.

Yamamuro, J. A. and Lade, P. V., (1999) "Experiments and modeling of silty sands susceptible to static liquefaction", Mechanics of Cohesive-Frictional Materials Vol. 4, No. 6, pp 545-564.

Yamamuro, J. A. and Covert, K. M., (2001) "Monotonic and cyclic liquefaction of very loose sands with high silt content", Journal of Geotechnical and Geoenvironmental Engineering Vol. 127, No. 4, pp 314-324.